ARTICLE

Investigating the effect of bentonite compaction density and environmental conditions on the corrosion of copper materials

Claire S. Tully[1] (ORCID) | **Wilfred J. Binns**[2] (ORCID) | **Dmitrij Zagidulin**[1] | **James J. Noël**[1,3]

[1]Department of Chemistry, Western University, London, Ontario, Canada

[2]Nuclear Waste Management Organization, Toronto, Ontario, Canada

[3]Surface Science Western, London, Ontario, Canada

Correspondence
James J. Noël, Department of Chemistry, Western University, 1151 Richmond St, London, ON N6G 2V4, Canada.
Email: jjnoel@uwo.ca

Abstract

The proposed long-term management plan for used nuclear fuel is to isolate it within a multiple-barrier system underground in a deep geological repository (DGR). In the Canadian design, used fuel bundles will be sealed in copper-coated carbon steel used fuel containers, encased in blocks of bentonite clay, emplaced approximately 500–800 m below ground, and surrounded by a bentonite gapfill material. A laboratory experimental campaign has been undertaken to demonstrate the integrity of the multiple-barrier system. DGR-relevant copper materials were embedded in bentonite clay, compacted to various densities, and sealed into a hermetic pressure vessel pressurized with demineralized water. Experiments explored the influence of bentonite compaction in the range of 1100–1600 kg/m^3 on copper corrosion over durations of 1–18 months. Postexposure analysis of the copper coupons showed nonhomogeneous corrosion, with corrosion products composed of Cu_2O, with some Cu_2S. The average corrosion rates decreased as a function of time and increasing bentonite compaction density. In general, we observed that higher bentonite compaction density suppressed the corrosion of embedded copper.

KEYWORDS
bentonite clay, compaction density, copper, corrosion, surface analysis, used fuel container

1 | INTRODUCTION

In Canada, the long-term management of used nuclear fuel is the responsibility of the Nuclear Waste Management Organization (NWMO). Per international best practice, the used fuel will be isolated within a multiple-barrier system underground within a stable host geological formation in a deep geological repository (DGR). In the proposed Canadian DGR design, used fuel bundles will be sealed in copper-coated carbon steel used fuel containers (UFCs), encased within blocks of highly compacted bentonite clay (HCB), and emplaced approximately 500–800 m below ground, depending on the host geology.[1] Gapfill material (GFM), a granulated bentonite product, will backfill any void space between the compacted bentonite blocks and the host rock walls.[1]

To receive a license to construct a DGR, the NWMO will need to demonstrate the long-term integrity and

safety of the DGR and the multiple-barrier system to the Canadian nuclear regulatory body as well as the local municipalities and Indigenous populations in the DGR siting region. To this end, the NWMO has undertaken extensive laboratory and in situ experimental programs to investigate the corrosion performance of copper materials in DGR-relevant conditions.[2–5] As part of this ongoing investigation, a series of exposure experiments on Cu in compacted bentonite clay exposed to various environments have been undertaken.

The stability of the UFC will be influenced by several environmental factors, including temperature, groundwater chemistry, pH, relative humidity, and potentially microbial activity, all of which will be influenced by the presence and state of the bentonite clay and will evolve over the lifetime of the DGR. At the time of emplacement of the Cu canisters, the DGR will be relatively cool (~20°C) with initial bentonite clay moisture contents of ~20% and ~5% in the HCB and GFM, respectively, and the environment will contain oxygen due to the air trapped during the emplacement process.[1,6] Based on a full-scale emplacement trial at the Mont Terri Underground Research Laboratory in Switzerland, conducted by the National Cooperative for the Disposal of Radioactive Waste (Nagra), the trapped oxygen is expected to be consumed within several months via mineral reactions with bentonite component minerals, microbial respiration, and minimal uniform UFC corrosion (~80 μm expected for the current Canadian DGR design).[1,6,7] Initially, the heat generated from the radioactive decay of the spent nuclear fuel within the UFC will drive water out of the bentonite toward the host rock, with resaturation occurring over approximately 20–1000 years, depending on the characteristics of the host geology (e.g., crystalline vs. sedimentary).[8] These changes in environmental conditions will also influence the activity of the microbes that are naturally found in bentonite clay, including sulfate-reducing bacteria (SRB).[9] Upon emplacement, the bentonite clay's water activity will be low, suppressing microbial activity. The effects of irradiation and increased temperature from the decaying fuel inside the UFC have also been shown to eliminate spore-forming bacteria below the detection limits of culturing.[10] Once the bentonite begins to wet from the host groundwater, the water activity will increase, with oxygen likely present, which may lead to viable microbial conditions during this transitory wetting process.[11] However, this remains partly dependent on the bentonite compaction density, as bentonite has been extensively shown to suppress microbial activity as a function of emplacement dry density.[5,12–14] The initial rate of wetting and eventual saturation of the bentonite clay has been shown to be dependent on the initial compaction density of the bentonite clay, which correlates to fewer macropores within the denser material.[15] Previous studies have found that the pore size distribution of the bentonite clay significantly changes as a function of bentonite wetting, which results in noncontinuous corrosion conditions for the UFC.[16] Oxygen will be depleted in the DGR through reactions on the UFC surface, potential aerobic microbial activity, and inorganic reactions with bentonite clay minerals and the host rock surface. The amount of trapped oxygen within the DGR will be partially determined by the compaction density of the HCB blocks and the GFM. Once depleted of oxygen, the DGR will remain anoxic for its operational lifetime. Under anoxic conditions, SRB, which is naturally found in bentonite clay, may become metabolically active should environmental conditions allow it. Through their metabolic pathway, they use sulfate as their terminal electron acceptor and generate sulfide, which can diffuse through the bentonite clay to the UFC surface and lead to the formation of Cu sulfide through microbially induced corrosion (MIC).

Due to bentonite's inhospitable physical and chemical properties, the number of culturable microbes in bentonite is very low, ranging from 10^2 to 10^3 colony-forming units per gram.[9] The low metabolic activity in bentonite clay is attributed partly to the high swelling pressure, low water activity, and small pore size. Previous studies determined that the number of metabolically active microbes decreases at higher bentonite dry densities. The transport of sulfide, either produced by the metabolic activity of microbes or present in low levels in the groundwater due to decaying organic matter or mineral dissolution, to the UFC surface will be controlled by diffusion through the bentonite clay. Previous research found that as the dry density of bentonite clay increases, the diffusion rate of sulfide decreases further, thereby decreasing the rate of sulfide supply to the surface of the UFC. From previous work, it was concluded that the dry bentonite dry density will play a significant role in the metabolic suppression of microbes and the diffusion of sulfide to the UFC. Through a series of experiments, this work aims to evaluate the overall effect of bentonite clay and Cu in a DGR-like environment. Cu materials were embedded in bentonite clay at various compaction densities and for different durations to evaluate the stability of Cu and the viability of microbes in the bentonite. Implications for the long-term performance of the proposed engineered barrier system for the long-term management of used nuclear fuel were then derived.

2 | MATERIALS AND METHODS

2.1 | Copper materials

Several Cu materials relevant to a Canadian DGR were investigated, which include cold-spray and electrodeposited Cu provided by the NWMO and oxygen-free, phosphorous-doped wrought Cu materials provided by the Swedish Nuclear Waste Management Organization, Svensk Kärnbränslehantering AB.[17] Cu coupons were machined to dimensions of approximately 1 cm × 1 cm × 3 mm. Before experiments, coupons were ground with silicon carbide papers with grits P180, P320, P600, P1200, P2500, and P4000 using Type I water as a lubricant. Coupons were then polished, using a 3 μm diamond suspension, rinsed with Type I water before being sonicated in 99% methanol and dried with an argon gas flow.

Coupons were stamped with a letter designating the Cu type followed by a numerical value to correlate the postexperiment sample to prerecorded mass and dimensions of the sample. Mass loss measurements were conducted following ASTM Standard G 31-21.[18] Coupons were weighed in triplicate with ±1 mg precision prior to each experiment. Following each experiment, coupons were extracted from the bentonite clay and rinsed with ethanol to remove residual bentonite, then the corrosion products were removed. Corrosion products were removed chemically by immersion in a deaerated solution of 1 M $HClO_4$ + 0.025 M hexamethylenetetramine ($C_6H_{12}N_4$), the latter to inhibit further corrosion. Residual corrosion products were removed by applying clear packing tape to the surface and then removing the tape with corrosion product residues attached. Coupons were then sonicated in methanol for 1 min and dried in a stream of argon gas. The mass lost by each coupon was then used to calculate a corrosion rate for each coupon, assuming uniform corrosion, by the following equation:[18]

$$\text{Average corrosion rate} = \frac{(K \times W)}{(A \times T \times D)}, \qquad (1)$$

where K is a constant of 8.76×10^7 to convert average corrosion rates into μm/year, W is the mass loss in grams to the nearest 1 mg, A is the area in cm^2 to the nearest $0.01\ cm^2$, T is the duration of exposure in hours, and D is the density of copper in g/cm^3.

Coupon dimensions before and following each experiment were measured to ±0.01 mm precision using a Vernier caliper. Before the coupons were placed in the bentonite pressure vessels for the experiment, photographs of each coupon's stamped face were taken; several coupons were also imaged using optical microscopy, scanning electron microscopy (SEM), and confocal microscopy to capture the condition of the pre-corroded surface for comparison.

2.2 | Pressure vessel assembly and disassembly

Copper coupons were loaded in pressure vessels containing Wyoming MX80 bentonite supplied by the NWMO; MX80 is a sodium-based bentonite with ~80% montmorillonite. The bentonite clay was subsequently compacted to 1100, 1400, or 1600 kg/m³ dry density with a custom hydraulic press. Figure 1 shows the experimental setup along with a schematic cross-section that illustrates the approximate position of each coupon. The moisture
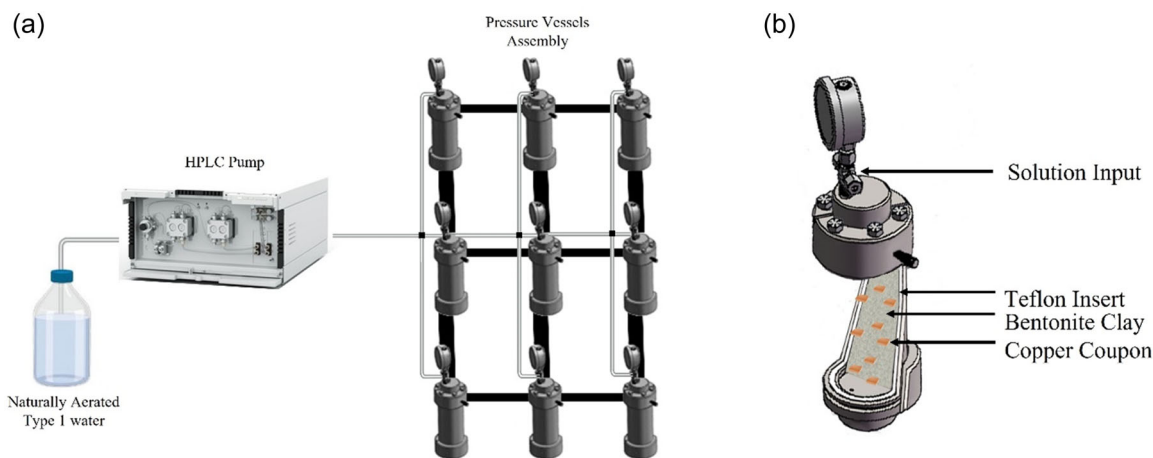

FIGURE 1 (a) Pressure vessel experimental setup along with a (b) schematic cross-section which illustrates the approximate position of each coupon. HPLC, high-performance liquid chromatography. [Color figure can be viewed at wileyonlinelibrary.com]

content of the received bentonite clay was calculated following ASTM Standard D2216-19. Briefly, a sample of bentonite clay is weighed, placed in an oven at 112°C for 24 h, and reweighed. The water content was determined through the following equation:[19]

$$w = \left[\frac{(M_{cms} - M_{cds})}{(M_{cds} - M_c)} \right] \times 100 = \left(\frac{M_w}{M_s} \right) \times 100, \quad (2)$$

where w is water content (%), M_{cms} is the mass of the container and moist specimen in grams, M_{cds} the mass of the container and oven-dried specimen in grams, s mass of the container in grams, s mass of water ($M_w = M_{cms} - M_{cds}$) in grams, and M_s is the mass of the oven-dried specimen ($M_s = M_{cds} - M_c$) in grams.

All bentonite used in this study was analyzed via culturing and 16S ribosomal RNA gene analysis before and after each experiment. These results are discussed in detail elsewhere but are important when analyzing the corrosion data.[11] Experiments were done in duplicate and for durations of 1–18 months.

The pressure vessel casings were fabricated from 316 stainless steel and had detachable stainless-steel filter stones lining the interior of the end caps. Each pressure vessel body was lined with a polytetrafluoroethylene inner casing, and all vessel components were sterilized by exposure to 99.5% (vol/vol) acetone and then to 70% (vol/vol) ethanol. Pressure vessels were assembled and disassembled on the benchtop using a hydraulic press and sterilized bentonite sampling tools. To accelerate the saturation of bentonite clay with water during the experiments, vessels were connected to an AZURA P6.1L high-performance liquid chromatography pump and constantly pressurized to 10 MPa with naturally aerated water from a Type I water system (Thermo-Scientific) with an initial resistivity of 18.2 MΩ cm for up to 18 months before being dismantled. Type 1 water is used in the current study to minimize the number of variables under study. Various chloride concentrations and simulated groundwater conditions are of interest and will be studied in future work and compared to these studies. Additionally, Type 1 water is a conservative bounding condition as salinities as low as 50 mg/L have been shown to inhibit bacterial growth. Aerated conditions are used to simulate the initial conditions of a DGR, which will contain oxygen from the atmosphere. A similar set of experiments starting from a deaerated condition are currently underway, which are more representative of long-term DGR conditions. Figure 2 shows the dismantling and sampling process. The bentonite plugs were cored to separate the inner bentonite from the outer bentonite, which was subsequently analyzed to determine its microbiological taxonomy, detailed in a separate publication.[10] The Cu coupons were removed from the outer region of the bentonite plugs and studied using a combination of microscopic and spectroscopic techniques to determine the extent of corrosion damage with respect to bentonite compaction density and time of exposure.

2.3 | SEM, energy-dispersive X-ray spectroscopy, and focused-ion beam analysis

Surface and cross-section morphologies of the corroded Cu samples were analyzed using a Hitachi SU3500 Variable Pressure SEM coupled to an Oxford AZtec X-Max50 SDD X-ray analyzer (EDX). For high-resolution imaging of focused-ion beam (FIB) cuts made by a LEO (Zeiss) 1540XB FIB/SEM using a gallium-ion beam, the Hitachi SU8230 Regulus Ultra High-Resolution Field Emission SEM coupled to the Bruker X-Flash FQ5060 Annular Quad EDX detector was used. For all instruments, an electron beam with an accelerating voltage ranging between 2 and 20 kV was used to collect high-resolution micrographs in secondary electron mode. EDX spectra were collected for a minimum of 5 min.

2.4 | X-ray photoelectron spectroscopy

The chemical state of corrosion products on the surface of coupons was determined using the Kratos AXIS Nova spectrometer X-ray photoelectron spectrometer (XPS) equipped with a monochromatic Al Kα X-ray source (hv = 1486.6 eV). Samples were loaded into the XPS using a detachable anaerobic chamber attached to the XPS loading chamber. High-resolution scans of the Cu LLM Auger peak were taken and fit using a Shirly background correction and fitted following the parameters determined by Biesinger.[20] The collected spectra were charge-corrected using the C 1s peak (corrected to 284.8 eV).

2.5 | Confocal laser scanning microscopy

The surface roughness of Cu coupons before and after experiments was mapped using a Zeiss LSM800/Zeiss Axio Imager Z2m upright compound microscope (CLSM) equipped with a 405 nm wavelength laser. The surface roughness values reported are the arithmetical mean height (S_a) values, which are absolute values measuring the height difference compared to the arithmetical mean of the surface.
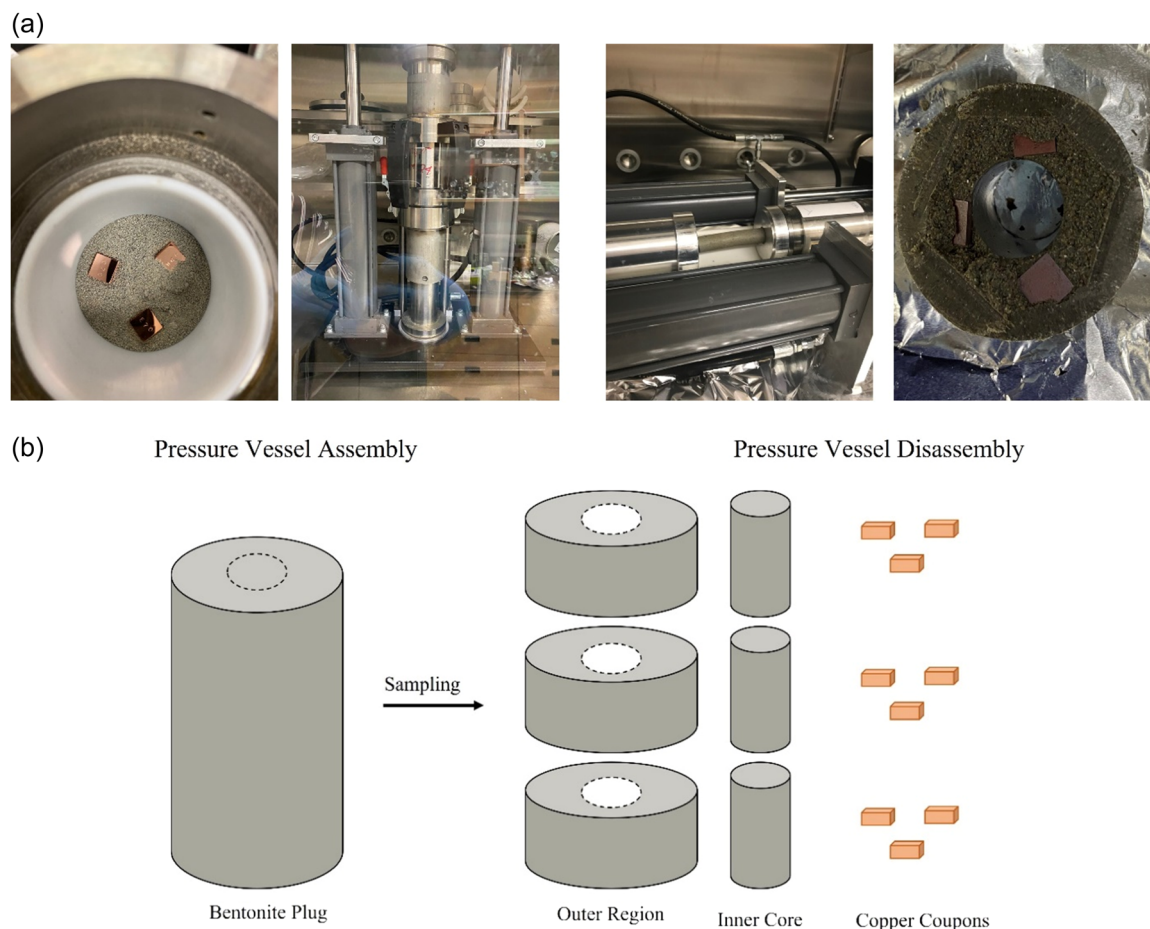
(a)

(b)   Pressure Vessel Assembly   Pressure Vessel Disassembly

FIGURE 2   Pressure vessel assembly and dismantling (a) and sampling (b). [Color figure can be viewed at wileyonlinelibrary.com]

3 | RESULTS AND DISCUSSION

3.1 | Saturation of the pressure vessels

The main mineral present in bentonite clay is montmorillonite, a smectite material capable of achieving high swelling pressures when compacted and hydrated. Due to the pore size variation, the bentonite clay's wetting and swelling are nonuniform. As a result, the saturation of bentonite in the pressure vessel depends on the clay's compaction, the chemistry of the solution, and time. In this study, we observed that pressure vessels, when pressurized from the top inlet, initiate two saturation fronts, one from the top and the other from the bottom. These fronts are visible in Figure 3, which shows a bentonite plug compacted to 1600 kg/m^3 that had been removed from a pressure vessel following a 1-month experiment. In this setup, the inlet water traveled along the polytetrafluoroethylene/stainless steel interface to the bottom of the pressure vessel and was then available to wet the clay from the bottom up, which was advantageous with respect to minimizing the time to saturation of the bentonite. By measuring the water activity of the various sections of the bentonite plug as a function of

time, it is possible to understand the required time to complete the saturation of each experiment. These measurements have been published elsewhere and show that the time required to achieve full saturation increases with the compaction density of the bentonite clay. While there is some variability in the results, complete saturation of pressure vessels containing bentonite compacted to 1100, 1400, and 1600 kg/m^3 appears to have occurred after approximately 1, 6, and 12 months, respectively. However, these approximate timelines are based on water activity measurements of bentonite, sampled following an experiment, and not on online saturation measurements and therefore are only coarsely quantitative. The copper specimens emplaced within the bentonite clay were therefore exposed to evolving conditions throughout the experiment as the wetting of the bentonite proceeded. When comparing compaction densities, it should be noted that the moisture content, pore size distribution, trapped oxygen, diffusion rates, and swelling pressures also vary, as vessels containing clay at lower compaction densities reach full saturation before those at the higher compaction densities and therefore have longer times of exposure to the saturated corrosion environment. This study provides insight into the corrosion

of UFC materials during initial wetting and saturation of the bentonite clay, which is indicative of corrosion under the conditions postemplacement when groundwater begins to saturate the bentonite clay.

3.2 | Corrosion product morphology

After the Cu coupons were extracted from the pressure vessels and the bentonite was removed, samples were

FIGURE 3 Saturation profile of a bentonite sample extracted from a pressure vessel. Bentonite was compacted to 1600 kg/m^3 for an experimental duration of 1 month. [Color figure can be viewed at wileyonlinelibrary.com]

analyzed using an optical microscope. In general, the optical micrographs obtained showed general, nonuniform corrosion, independent of Cu form, bentonite compaction density, or duration of exposure. Two representative optical micrographs of a cold-spray Cu embedded for 12 months in bentonite compacted to 1400 kg/m^3 are shown in Figure 4. The Cu surface was a heterogeneous mixture of underlying matte Cu unevenly covered in pale and dark gray surface layers. In the higher-resolution image, small red and blue features can be seen decorating the gray surface layers. These features were likely a mixture of corrosion products and bentonite that was not thoroughly cleaned from the surface. The fact that such an irregular surface existed is not surprising, given the presence of the saturated bentonite, which would wet the Cu surface slowly and nonuniformly over time.

The morphology of the corrosion products on the Cu surface was imaged using SEM. The observed surface did not show extensive corrosion after 7 months of exposure to water-saturated bentonite clay. The increased exposure time led to the formation of multiple shallow defects and surface roughening in specific areas; however, the presence of bentonite and corrosion products prevented us from investigating the whole surface. In the regions with increased surface roughness and shallow defects, elemental maps showed increased amounts of silicon, aluminum, and oxygen, likely associated with bentonite clay being more firmly adhered to the Cu surface. Figure 5 shows cold-spray Cu embedded in bentonite compacted to 1400 kg/m^3 for 1, 3, and 7 months with EDX spot analysis at two locations on the surface of the 7-month sample, which further suggests nonhomogenous corrosion morphology on the Cu surface. Profilometry of coupon surfaces using CLSM was also performed on samples after the corrosion product was removed from the surface following each experiment. Representative micrographs are shown in Figure 6 for coupons embedded in bentonite compacted to 1400 kg/m^3 for 1, 4, and 12 months. Over this timeframe, there was a
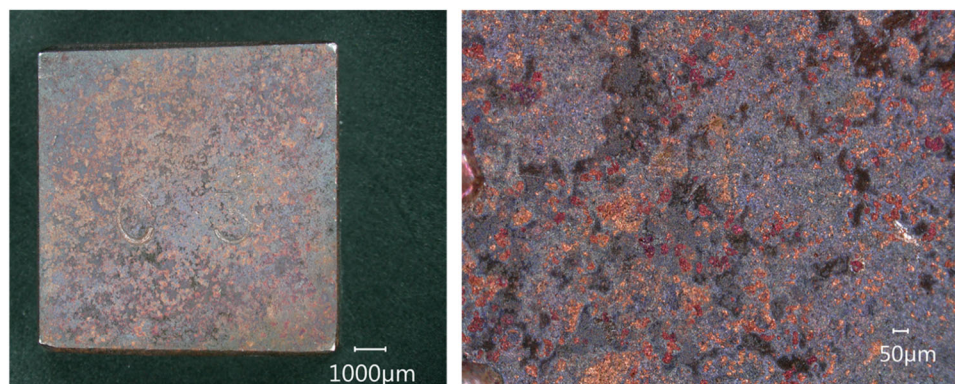

FIGURE 4 Optical image of cold-spray copper sample corroded in 1400 kg/m^3 bentonite clay for 12 months. [Color figure can be viewed at wileyonlinelibrary.com]

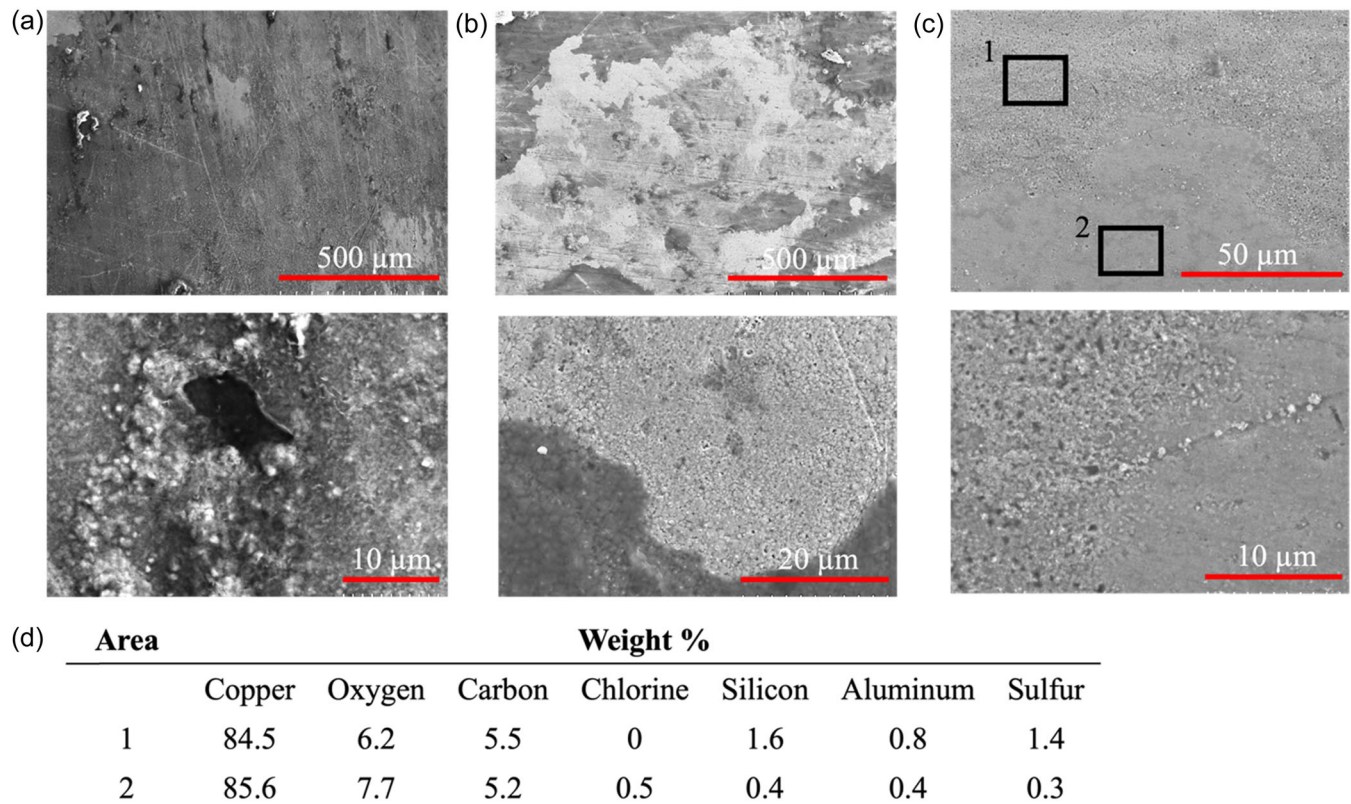| Area	Weight %						
	Copper	Oxygen	Carbon	Chlorine	Silicon	Aluminum	Sulfur
1	84.5	6.2	5.5	0	1.6	0.8	1.4
2	85.6	7.7	5.2	0.5	0.4	0.4	0.3

FIGURE 5 SEM micrographs of cold-spray copper samples corroded in 1400 kg/m^3 bentonite clay for (a) 1 month, (b) 3 months, and (c) 7 months with elemental mapping of sample (c) shown in (d). SEM, scanning electron microscopy. [Color figure can be viewed at wileyonlinelibrary.com]

Experiment Duration	1 month	4 months	12 months
Surface Roughness (Sa)	0.79 μm	0.99 μm	1.6 μm
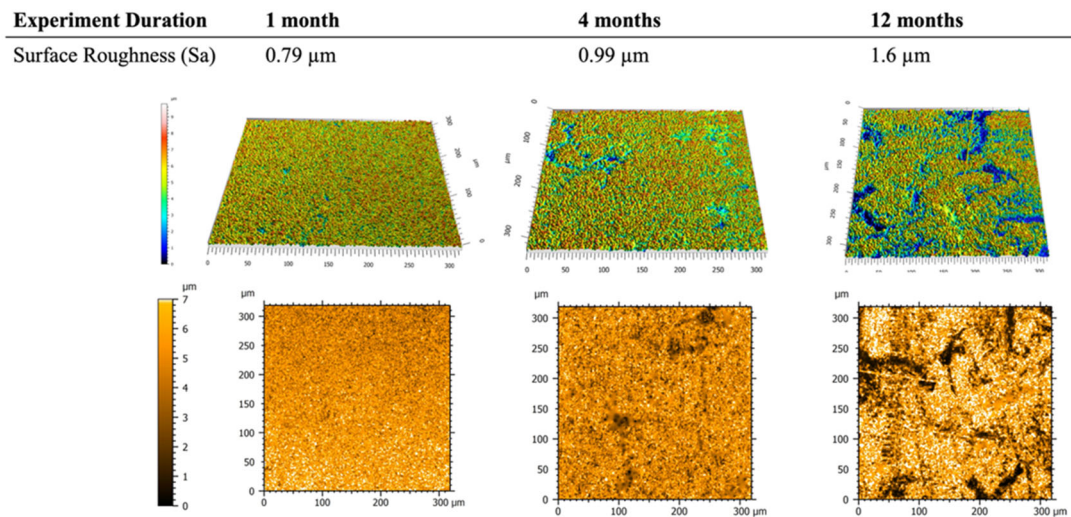
Cold-spray copper corroding in bentonite clay compacted to a dry density of 1400 kg/m^3 for various durations

Duration	Surface Roughness	Standard Deviation
1 month	0.77 μm	0.03 μm
4 months	1.0 μm	0.01 μm
12 months	1.17 μm	0.60 μm

FIGURE 6 Confocal three-dimensional maps of cold-spray copper materials corroded in 1400 kg/m^3 bentonite clay for 1, 4, and 12 months. [Color figure can be viewed at wileyonlinelibrary.com]

slight increase in the measured surface roughness of the samples from 0.77 to 1.17 µm. however, these measurements are not distinguishable within error.

The corrosion product thickness, morphology, and composition were further investigated using SEM/FIB cuts combined with EDX analysis. FIB cuts were taken through areas with a bentonite deposit adhered to the Cu surface to ensure that intact corrosion product films were analyzed.

In some cases, a layer of silver was deposited on the surface before FIB milling to prevent the corrosion product from being damaged by the cutting beam. Figure 7 shows a SEM micrograph of a FIB cut of two cold-spray samples embedded for 4 and 7 months in bentonite with a density of 1400 kg/m^3. Qualitatively, there was no increase in the corrosion product thickness on the surface of cold-spray copper from the 4-month to the 7-month exposure time. However, in the 4-month experiment, the Cu corrosion product appeared more porous than the compact corrosion product formed after

7 months of exposure. This could have been due to the increase in swelling pressure as the bentonite clay wetted and subsequently swelled, exerting pressure on the corrosion product film and causing it to become more compact. This is speculative, but experiments to correlate such phenomena with online measurements of bentonite saturation/swelling are currently underway. Regardless of bentonite dry density or experimental duration, EDX spectroscopy confirmed the presence of Cu, oxygen, and sulfur in the corrosion products on each sample surface. EDX elemental mapping revealed the Cu and oxygen to be distributed throughout the corrosion product layer, with sulfur typically present in the outermost layer of the corrosion product and in areas of damage under the corrosion product, as shown in Figure 7c. This observation is consistent with the conversion of a pre-existing Cu_2O film (either from air exposure or oxygen-induced corrosion during the early stages of the experiment) to Cu_2S upon exposure to HS^-, which would be expected in a DGR environment.[21–23]
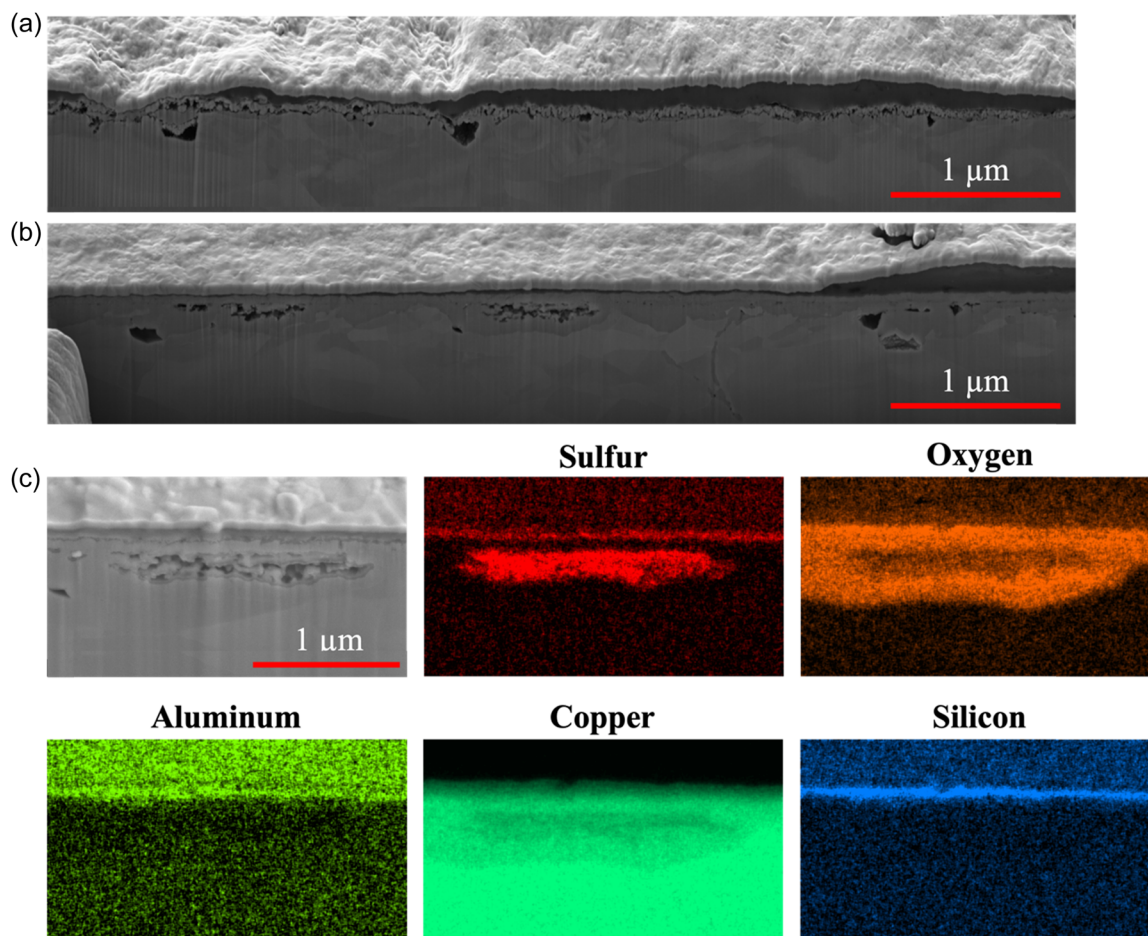

FIGURE 7 SEM micrographs of cold-spray copper samples corroded in 1400 kg/m^3 bentonite clay for (a) 4 months and (b) 7 months. (c) Elemental mapping of the corrosion product by EDX is shown in (b). SEM, scanning electron microscopy, EDX, energy-dispersive X-ray analysis.

While the change in experimental duration from 4 to 7 months did not affect the corrosion product thickness or composition significantly, the same could not be said for the bentonite compaction density. Figure 8a,b shows SEM micrographs of FIB-cut cold-spray Cu samples embedded in bentonite compacted to 1100 and 1400 kg/m^3, respectively, which were exposed to Type I water for 6 months, with the corresponding EDX elemental maps in Figure 8c,d. Again, Cu and oxygen were dispersed throughout the corrosion product, with sulfur enriching the outermost layer. However, in the lower bentonite density experiment, a significantly thicker sulfur layer of approximately 500 nm was present on the outermost portion of the corrosion product. This was five times thicker than the sulfur layer present on the Cu coupon from the experiment conducted at 1400 kg/m^3 compaction. The greater thickness of the Cu_2S layer could have been due to increased microbial activity in the lower-density bentonite, or it could have been related to the faster saturation time of the lower-density bentonite, leading to the release of sulfide from the dissolution of minerals within the bentonite itself. Microbiological analysis of the bentonite used in this study did not find significant SRB growth in any of the bentonites studied; therefore, MIC was not suspected. However, SRB activity may have occurred elsewhere in the pressure vessel,

providing a source of sulfide; for example, the interface of the bentonite clay and the filter stone may have provided a more hospitable condition. However, the sulfide source in the corrosion product layer has not yet been determined. At higher compaction densities, we observed more compact corrosion product deposits, thinner than those produced at lower compaction densities. This may have been due to the increased swelling pressure and the restricted and delayed bentonite wetting compared to the experiments with lower bentonite densities. We observed an increase in the amount of sulfide on the Cu surface in the lower bentonite compaction experiments, suggesting that the density of the bentonite significantly influenced the mobility of the sulfide species and/or the microbial metabolic activity that can produce sulfide species.

Figure 9 shows FIB cuts on wrought and cold-spray copper, taken 3 and 6 months after exposure to bentonite compacted to 1100 kg/m^3. At low bentonite compaction densities, for both wrought and cold-spray Cu materials, the corrosion products formed after 1 month appear to have been a uniform corrosion layer, with oxygen and Cu being dominant in the corrosion product and some sulfur being present at the corrosion product/bentonite interface. However, after 6 months of exposure, the morphology of the corrosion product appeared porous, with increased sulfur corrosion product thickness.
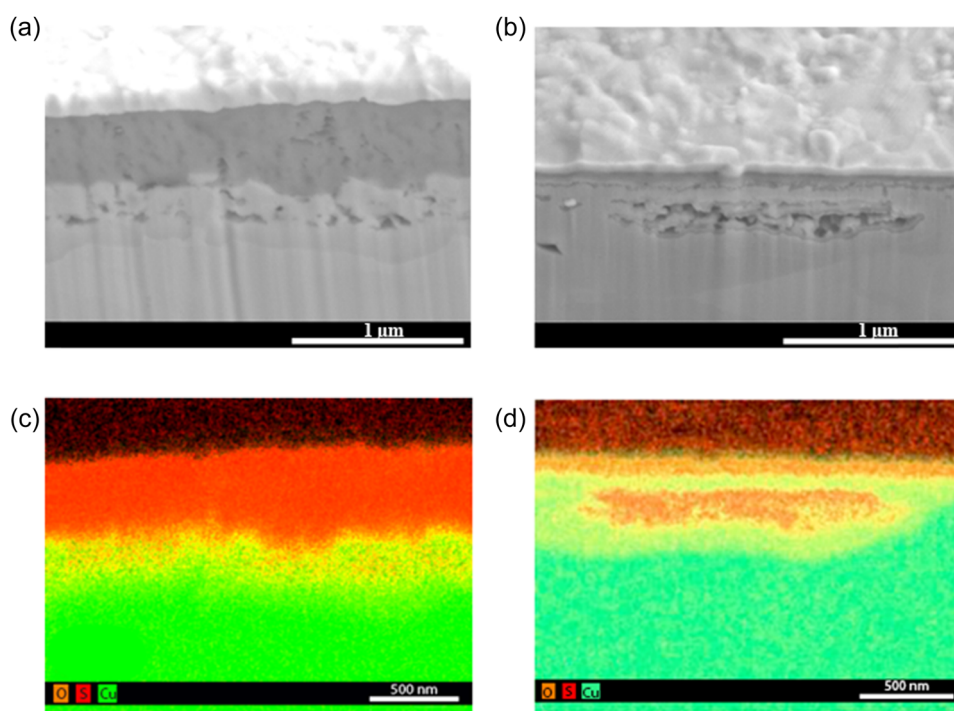

FIGURE 8 SEM micrograph of FIB cut of a cold-spray sample exposed to saturated bentonite with a dry density of (a) 1100 kg/m^3 and (b) 1400 kg/m^3 for 6 months with corresponding elemental maps of copper, oxygen, and sulfur signals. FIB, focused-ion beam; SEM, scanning electron microscopy. [Color figure can be viewed at wileyonlinelibrary.com]
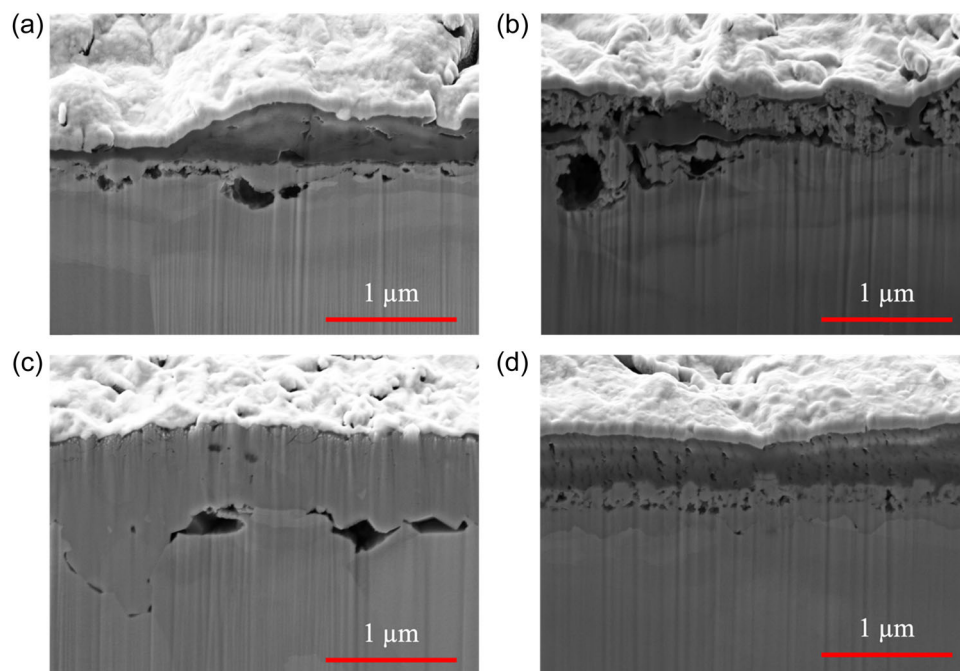
FIGURE 9 (a) FIB cut of a wrought copper sample exposed to saturated compacted bentonite clay for 3 months and (b) 6 months; (c) FIB cross section of a cold-spray copper sample exposed to the saturated compacted bentonite clay for 3 months and (d) 6 months. In all cases, bentonite dry density was 1100 kg/m^3. FIB, focused-ion beam. [Color figure can be viewed at wileyonlinelibrary.com]

3.3 | Corrosion product composition

The chemical states of the corrosion products existing on cold-spray Cu following pressure cell experiments of up to 12 months duration in bentonite compacted to 1400 kg/m^3 were determined using XPS, shown in Figure 10. Using the copper Auger peak, we found that the dominant corrosion product formed (i.e., ~60 atom%) was Cu$_2$O, likely formed during sample preparation and corrosion due to trapped oxygen in the system. Additionally, we detected Cu$_2$S, typically around 35 atom%, which would have formed under anoxic conditions with a sulfide source, along with some CuSO$_4$. While the full experimental matrix is not yet complete, very little difference has been seen between the experiments conducted to date with respect to the composition of the corrosion product layers. This is despite the large differences in the time-to-saturation as a function of compaction density, which can differ by about 11 months from the low to the high densities tested, as described in Section 3.1. In all cases, the evidence suggested that there was an initial period of oxic corrosion, which was succeeded by a short period of sulfide production, leading to Cu$_2$O conversion to Cu$_2$S at the outer surface of the Cu. The mechanism by which the sulfide was generated is not currently understood and will be the subject of future work. It should also be noted that XPS analysis
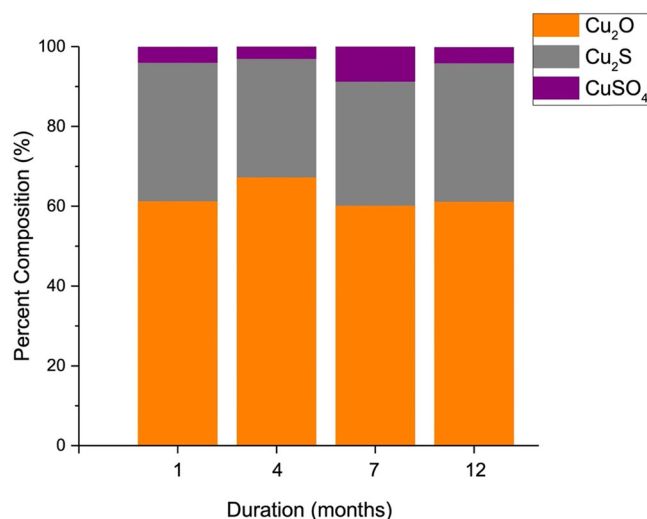

FIGURE 10 Percent composition of the corrosion product formed on cold-spray copper when embedded for various durations in bentonite clay compacted to 1400 kg/m^3. XPS of Cu LLM peak was fitted using Casa XPS software (Shirley baseline corrosion). XPS, X-ray photoelectron spectrometry. [Color figure can be viewed at wileyonlinelibrary.com]

only probes the top ~5 nm of the sample surfaces, and so these data must be taken in the context of the other surface analyses and corrosion rate measurements conducted in this work.

3.4 | Average corrosion rates

The average corrosion rate of Cu coupons extracted from the pressure vessels containing bentonite compacted to 1100, 1400, and 1600 kg/m3 after exposure for up to 12 months was determined through mass loss measurements, and the results are shown in Figure 11. It should be noted that such mass loss calculations assume uniform corrosion of the Cu surface, which is well justified given the absence of localized corrosion in the surface analysis. In all cases, the average corrosion rates showed the same overall trend: a steep decline in corrosion rate over the first 4 months, followed by a slow decline of corrosion rate to under $1 \mu m$/year after about 175 days. Such results are in line with other studies of Cu embedded in bentonite and Cu immersed in anoxic brines.[24,25] Coupons embedded in bentonite compacted to lower densities showed initial average corrosion rates higher than those measured in higher-density experiments, with ranges of 7.5–8.5, 6.0–6.5, and 0.4–1.9 μm/year for experiments conducted in bentonite with dry densities of 1100, 1400, and 1600 kg/m^3, respectively. This discrepancy in initial corrosion rates could have been due to a few factors, including: increased pore space in lower-density pressure vessels, which would have initially contained more oxygen leading to corrosion; faster time to saturation, leading to a greater proportion of trapped oxygen, causing corrosion as opposed to other consumption routes, such as microbial respiration or mineral reactions; or increased MIC, due to the lower swelling pressure of less-dense clay. Concerning Cu, there was no apparent difference between the cold-spray,
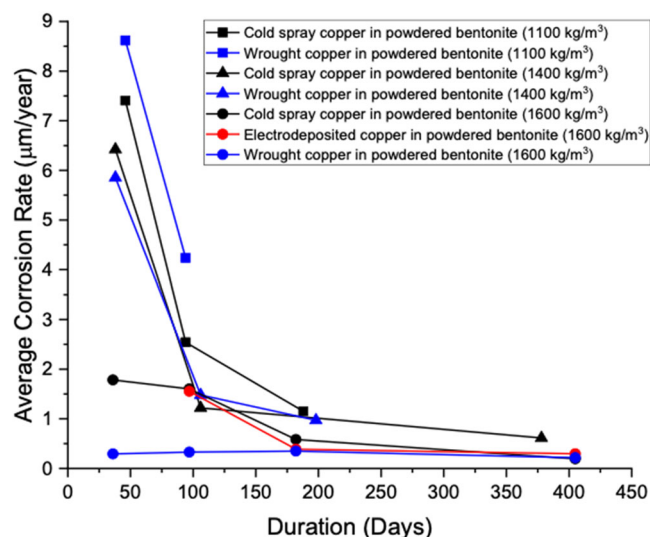
electrodeposited, or wrought Cu materials tested, which is in line with previous work evaluating these materials in DGR-like conditions.

While the data presented in this paper are not complete, some clear trends and processes are emerging. The initial oxidation of the Cu specimens is due to the presence of oxygen within the bentonite pores, leading to the formation of a thin Cu_2O corrosion product layer. From mass loss measurements, this process is anticipated to occur over approximately the first 100 days of the experiments, which is evident in Figure 11, where there was a steep decline in corrosion rates. Calculations were performed to quantify the amount of oxygen that would have been trapped in the initial pore voids, the initial moisture within the bentonite clay, and the input of naturally aerated Type-I water. Calculations for determining the amount of available oxygen resulted in the approximation of 6×10^{-3} moles of available oxygen, with 3 mol of O_2 available per square metre of the copper surface.[6] Assuming all oxygen was consumed on the Cu surface, that would result in a maximum of 0.05 mm of corrosion damage, assuming no oxygen was consumed through reactions with the bentonite clay or from microbial activity, which is not the case. The amount of trapped oxygen within the pressure vessels was largely that trapped in the pore void when assembled with low amounts of oxygen being introduced during pressurization. From FIB cuts, we see a maximum of $1 \mu m$ in corrosion product thickness, assuming Cu_2O to Cu_2S conversion, which would lead to the consumption of 0.0001 moles of oxygen. As a result, the estimated amount of oxygen used in the corrosion of the Cu coupons is approximately 2% of the total trapped oxygen. This calculation is conservative, as it does not discount the initial oxide from sample preparation. After the oxic period, the pressure cell environment was anoxic, as indicated by the small amount of sulfide-induced corrosion that appeared to have occurred, given the EDX and XPS data in Figures 7–9. While it is not clear whether the source of this sulfide was microbiological or inorganic, from the dissolution of the bentonite minerals (a companion study by Beaver et al.[11] does not provide evidence of SRB growth), it is clear that this process was prolonged, leading to submicrometer per year rates of corrosion. It may be that corrosion ceased in these experiments, as mass loss measurements do not provide instantaneous corrosion rates but averaged corrosion rates over the entire experimental duration. More experiments of longer duration are currently underway to resolve this. It is also clear from this work that the dry density of the emplaced bentonite does influence the initial corrosion rates (i.e., lower density leads to a higher initial corrosion rate) but that this effect fades with time,

FIGURE 11 Average corrosion rates of Cu material embedded in bentonite clay at various densities. [Color figure can be viewed at wileyonlinelibrary.com]

leading to uniform corrosion rates of less than 1 μm/year beyond about 200 days. Finally, the form of the Cu material (cold-spray vs. electrodeposited vs. wrought) does not significantly affect the observed corrosion rates.

3.5 | Copper diffusion through bentonite clay

During the corrosion process, Cu species diffused through the bentonite clay into the bulk material. Figure 12 shows a cross-section of a piece of bentonite clay that was previously in contact with a cold-spray Cu coupon for 1 month at a bentonite compaction density of 1100 kg/m^3. The bentonite clay was extracted from the pressure vessel, impregnated with epoxy (as indicated by the strong carbon signal), and polished to a 3 μm finish using silica-based lubricants. The sample was then coated in platinum to increase conductivity. Although we observed a diffusion gradient of Cu species into the bulk bentonite clay, we expected the Cu species to be in an anionic state, due to the cation exchange properties of the bentonite clay.

In some cases, when Cu coupons were removed from the bentonite clay, significant red staining was noted at the Cu/bentonite interface. The cross-section of the bentonite clay revealed a blue discoloration that was most vibrant at the Cu bentonite interface, with color intensity following the diffusion gradient. This diffusion gradient was only observed at bentonite dry densities of 1100 kg/m^3 at all durations and, in some cases, 1400 kg/m^3 after 6 months. This was likely the result of changes in porosity due to compaction density decreasing the diffusion rates of Cu species within the bentonite material.

4 | CONCLUSIONS

We observed a decrease in the average corrosion rates of Cu materials over time in the presence of bentonite clay and the influence of bentonite compaction on the corrosion of Cu materials. The average corrosion rates of the Cu materials were initially elevated, then decreased exponentially with time. We expect that the initially higher corrosion rates resulted from trapped oxygen within the pressure vessel and the oxygen found in the naturally aerated solution used to wet the bentonite clay. We suspect that oxygen depleted over time, which led to a decrease in the average corrosion rates. The higher-density experiments had a smaller volume of trapped oxygen; this oxygen can react with the bentonite clay and limited microbial communities, as well as the Cu materials, resulting in a Cu oxide layer at the surface thinner than that observed in experiments with lower-density bentonite. That oxygen depleted from the system was supported by the presence of Cu sulfides and sulfur species on the outermost layer of the corrosion
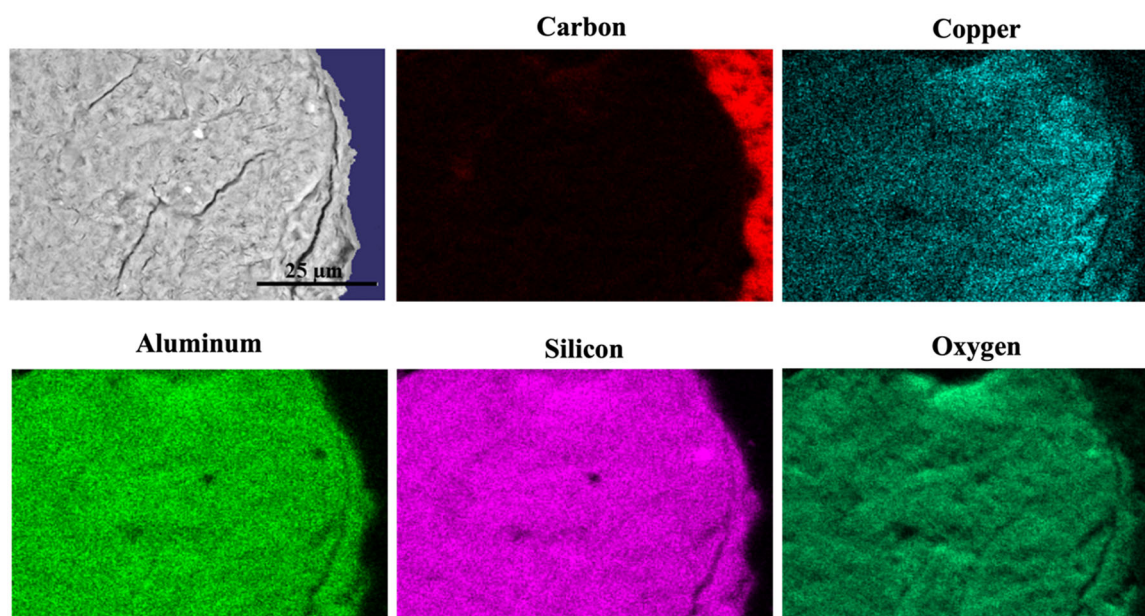

FIGURE 12 SEM micrograph and EDX elemental mapping of a bentonite cross-section that was in contact with a corroding cold-spray copper sample for 1 month and compacted to a dry density of 1100 kg/m^3. EDX, energy-dispersive X-ray analysis; SEM, scanning electron microscopy. [Color figure can be viewed at wileyonlinelibrary.com]

product, suggesting the formation of Cu oxides followed by a conversion to Cu sulfide once the environment became anoxic.

The higher compaction density of the clay also resulted in higher swelling pressures, which appeared to influence the corrosion product morphology and resulted in a more compact corrosion product. At higher clay densities, we also observed a thinner layer of Cu sulfide species at the Cu oxide/bentonite interface, indicating either the suppression of microbially produced sulfide species and/or a decrease in the diffusion rates of the sulfide species to the Cu materials. From surface profilometry and morphology measurements, we continued to see an increase in surface roughening over time, suggesting that while the average corrosion rates were low, the Cu materials were still corroding at very low rates.

ACKNOWLEDGMENTS

DATA AVAILABILITY STATEMENT

Research data are not shared.

ORCID

Claire S. Tully 🔟 http://orcid.org/0000-0001-7736-4417
Wilfred J. Binns 🔟 https://orcid.org/0000-0003-2472-1251

REFERENCES

[1] D. S. Hall, M. Behazin, W. Jeffrey Binns, P. G. Keech, *Prog. Mater. Sci.* **2021**, *118*, 100766.

[2] P. G. Keech, M. Behazin, W. J. Binns, S. Briggs, *Mater. Corros.* **2021**, *72*, 25.

[3] J. R. Scully, D. Féron, H. Hänninen, NWMO TR-2013-04, Nuclear Waste Management Organization, Toronto, Canada **2013**.

[4] J. R. Scully, D. Feron, H. Hanninen, *TR 2016-11*, Nuclear Waste Management Organization, Toronto, Canada **2016**.

[5] D. S. Hall, P. G. Keech, *Corros. Eng., Sci. Technol.* **2017**, *52*, 2.

[6] D. S. Hall, T. E. Standish, M. Behazin, P. G. Keech, *Corros. Eng., Sci. Technol.* **2018**, *53*, 309.

[7] N. Giroud, Y. Tomonaga, P. Wersin, S. Briggs, F. King, T. Vogt, N. Diomidis, *Appl. Geochem.* **2018**, *97*, 270.

[8] T. L. Rashwan, M. A. Asad, I. L. Molnar, M. Behazin, P. G. Keech, M. M. Krol, *Sci. Total Environ.* **2022**, *828*, 153944.

[9] M. A. Vachon, K. Engel, R. C. Beaver, G. F. Slater, W. J. Binns, J. D. Neufeld, *Sci. Rep.* **2021**, *11*, 22349.

[10] K. Pedersen, M. Motamedi, O. Karnland, T. Sandén, *Eng. Geol.* **2000**, *58*, 149.

[11] R. C. Beaver, M. Vachon, C. S. Tully, K. Engel, E. Spasov, W. Binns, J. J. Noël, J. Neufeld, *J. Appl. Microbiol.* **2023**.

[12] K. Pedersen, A. Bengtsson, A. Blom, L. Johansson, T. Taborowski, *Appl. Clay Sci.* **2017**, *146*, 495.

[13] S. Stroes-Gascoyne, C. J. Hamon, P. Maak, S. Russell, *Appl. Clay Sci.* **2010**, *47*, 155.

[14] K. Pedersen, *J. Appl. Microbiol.* **2010**, *108*, 1094.

[15] Q. Wang, Y. J. Cui, A. Minh Tang, L. Xiang-Ling, Y. Wei-Min, *Soils Found.* **2014**, *54*, 657.

[16] P. Delage, D. Marcial, Y. J. Cui, X. Ruiz, *Géotechnique* **2006**, *56*, 291.

[17] W. Li, B. Yu, J. Tam, J. D. Giallonardo, D. Doyle, D. Poirier, J. G. Legoux, P. Lin, G. Palumbo, U. Erb, *Surf. Coat. Technol.* **2020**, *532*, 152039.

[18] ASTM G 31, *Standard Guide for Laboratory Immersion Corrosion Testing of Metals*, Vol. 72, **1999**, p. 1.

[19] ASTM-D-2216-98, *Standard Test Method for Laboratory Determination of Water (Moisture) Content of Soil and Rock by Mass*, **1998**, p. 1.

[20] M. C. Biesinger, *Surf. Interface Anal.* **2017**, *49*, 1325.

[21] J. M. Smith, J. C. Wren, M. Odziemkowski, D. W. Shoesmith, *J. Electrochem. Soc.* **2007**, *8*, 154.

[22] J. H. Stenlid, A. J. Johansson, C. Leygraf, T. Brinck, *Corros. Eng., Sci. Technol.* **2017**, *52*, 50.

[23] M. Guo, J. Chen, C. Lilja, V. Dehnavi, M. Behazin, J. J. Noël, D. W. Shoesmith, *Electrochim. Acta* **2020**, *362*, 137087.

[24] N. A. Senior, R. C. Newman, D. Artymowicz, W. J. Binns, P. G. Keech, D. S. Hall, *J. Electrochem. Soc.* **2019**, *166*, C3015.

[25] N. A. Senior, T. Martino, J. W. Binns, P. G. Keech, *Mater. Corros.* **2021**, *72*, 282.